

Dynamics of OH masers in regions of star formation I

T. Thissen, H. Spiecker, and P. Andresen

Angewandte Laserphysik, Universität Bielefeld, Universitätsstr. 25, D-33615 Bielefeld, Germany

Received August 13, 1998; accepted March 22, 1999

Abstract. A mathematical model for the explanation of OH masers in regions of star formation is presented. The model is based on the assumption that grains of different sizes are present at the border of the HII regions where they are exposed to the heat- and VUV-flux of a new born star. The grains evaporate water because of the heat flux from the central star. The subsequent dissociation of water by VUV together with IR relaxation generates a high OH abundance and yields strong inversion in the OH Λ -doublets for all maser transitions observed in star forming regions. The gain of the observed masers is determined as a function of the photodissociation rates for different evaporation rates. In this first approach IR pumping and collisions are neglected although they may change the quantitative predictions. The results show that gain may be high enough to explain all observed masers near new born stars under reasonable assumptions for the astrophysical conditions found at the border of HII regions. Based on the model predictions are made concerning intensities, locations and variability of the different maser transitions.

Key words: ISM: OH — masers — hyperfine population — W3(OH) — photodissociation — HII regions

1. Introduction

The present study about the origin of OH maser radiation near new born stars was motivated by a recent study by Baudry & Diamond (1998) on the $^2\Pi_{3/2}(j = 7/2)$ 13.44 GHz OH maser emission in W3(OH). This study was done with high spatial resolution and revealed a pronounced spatial structure with filaments containing single

small and very intense maser spots. The compact area in which all of the $j = 7/2$ masers are observed is very close to the maximum of 23.8 GHz continuum emission, which is suspected to be the position of a massive new born star (Baudry & Diamond 1998). There is one spot that extends over only 1 astronomical unit (AU) and yields a microwave flux of more than 20 Jy on earth. Because the bandwidth is $\Delta\nu \approx 10$ kHz the observed line integrated flux density from this spot is $j_{\text{obs}} \approx 2 \cdot 10^{-21} \text{ W/m}^2$. A general background emission of 20 mJy is observed from the whole area where OH $j = 7/2$ masers are found. The 13.44 GHz masers operate between the two Λ -doublet states of the $j = 7/2$ rotational level in the $^2\Pi_{3/2}$ multiplet state of OH between the $F = 4$ hyperfine states.

Because the maser emission originates from a rotationally excited state in OH with a high IR relaxation loss rate of $\approx 0.5 \text{ s}^{-1}$ a very efficient mechanism must pump OH molecules into the $j = 7/2$ state to account for the high loss rate. Despite this high loss rate the maser emits a large photon flux. Baudry & Diamond (1998) discuss the observations on the currently available maser models which assume collisional and/or IR pumping schemes (e.g. Elitzur 1992) including radiation transport. For the excitation of the high lying maser in the $j = 7/2$ state the observations are extremely difficult to explain by these models. Baudry & Diamond (1998) speculate that a shock might excite the maser. However, although the shock should show up in the data, it is not seen. Here we try to explain this maser radiation by a completely different mechanism, based on grains that evaporate water in the presence of VUV which photolyzes water in the first absorption band creating inversion in the nascent OH photoproduct. This fundamental mechanism was not even mentioned by Baudry & Diamond (1998) although it has been suggested almost 15 years ago (Andresen 1985).

In this paper we will work out a quantitative OH maser model including evaporation of water from grains, generation of OH by the photodissociation of water, subsequent IR relaxation and destruction of OH by photolysis. We will show that this model yields population inversion and

Send offprint requests to: T. Thissen,
e-mail: tthissen@physik.uni-bielefeld.de

Correspondence to: Fakultät Physik, Universität Bielefeld,
Universitätsstr. 25, D-33615 Bielefeld, Germany.

gain for all masers observed in star forming regions. In this still crude model we neglect collisions and FIR-pumping, which will affect the population to some extent, in particular at low photodissociation rates. We give quantitative numbers for the gain for the different maser transitions as a function of photodissociation and evaporation rates. It is interesting to note that all masers can operate over a wide range of photodissociation rates and that the output is determined to a larger extent by the evaporation rate rather than by the photodissociation rate. Nevertheless there are some OH maser features which cannot be explained with our model up to now, e.g. the absorption line at 13434 MHz or the 1667 MHz/1665 MHz emission ratio. Therefore we are working on various aspects to improve the present model. One aspect is the inclusion of FIR pumping and collisions, others are related to steric effects. We will show that collisions can be neglected at high photodissociation and IR relaxation rates.

We also elaborate on the astrophysical conditions required for the application of the present maser model. In contrast to the maser models discussed by Baudry & Diamond (1998), which do not even explain the origin of the high OH abundance, we use the well accepted picture of star formation in which the star is surrounded by a large cloud of grains. We will show that grains at the border between the HII region and the cold cloud are exposed to the heat- and VUV- flux from the central star and that in this situation masing should occur. We discuss the role of different grain sizes on the evaporation. The present model predicts that OH maser radiation should occur whenever grains are exposed to the heat flux and the VUV flux from the central star.

According to the present model ground state OH masers should be located directly at the border between the HII region and the grains. We will also discuss under which conditions the present maser model might explain the very high flux density obtained from the small diameter spot observed by Baudry & Diamond (1998) for the 13.44 GHz maser.

2. Generation and population of OH

In this section the generation of OH through photodissociation of water evaporated from grains in the radiation field of a new born star is investigated. Details about the evaporation process are given in Sect. 3.

Here we assume that grains are exposed to the heat flux from the star and will evaporate water. The term heat flux describes the total amount of energy from the star which heats the grains either by direct absorption or indirect absorption (e.g. photolytic heating). The evaporated water will be photolysed and yield OH with a peculiar nascent distribution over different quantum states. The continued formation and relaxation yields inversion between all those quantum states between which masing has

been observed in star forming regions. The OH quantum state distribution presented here might also be affected by the absorption of FIR radiation from the surrounding dust and the reabsorption of the OH rotational lines which are emitted after photolysis of water because OH is formed in rotationally excited states. Because of the difficulties in quantifying these effects, they are excluded up to now. Nevertheless we think that the photodissociation and the subsequent IR relaxation will dominate the quantum state population at least under certain conditions, e.g. at high photodissociation rates. For the ground state masers the FIR pumping may play a more important role than for the excited state masers.

The evaporation from the grains is described by the evaporation rate Γ , i.e., the number of water molecules desorbed from grains per m^3 and second. In the evaporation process water molecules go off the grains to the gas phase, which implies that the grain size decreases with time.

In the gas phase the water molecules are photolysed in the VUV radiation field with a photodissociation rate γ_1 . The nascent OH is formed in different quantum states with a probability f_i for state i . The nascent quantum state population in OH relaxes subsequently by IR emission towards lower states with IR relaxation rates A_{ik} . There is an interesting competition between photodissociation and IR relaxation which depends on the photodissociation rate. The OH is also photolysed in the VUV radiation field with a photodissociation rate γ_2 , which presents the only loss mechanism for ground state OH in the present model. The corresponding maser model is shown in Fig. 2.

Grains: For a quantitative model, we consider a 1 m^3 volume of the maser with water containing grains of radius r_{gr} . The effects of different grain radii are discussed in Sect. 3. A grain with radius r_{gr} has a surface area $A_{\text{gr}}(r_{\text{gr}})$ and a volume $V_{\text{gr}}(r_{\text{gr}})$. Although grains are expected to have a porous structure we assume spherical grains with $A_{\text{gr}} = 4\pi \cdot r_{\text{gr}}^2$ and $V_{\text{gr}} = 4/3\pi \cdot r_{\text{gr}}^3$ for simplicity.

The density of the grains with radius r_{gr} (number of grains of that radius per m^3) is denoted by $n_{\text{gr}}(r_{\text{gr}})$. From the number $n_{\text{gr}}(r_{\text{gr}})$ of grains with radius r_{gr} and their surface $A_{\text{gr}}(r_{\text{gr}})$ we calculate the grain surface area contained in 1 m^3 of the maser volume by $O_{\text{gr}}(r_{\text{gr}}) = n_{\text{gr}}(r_{\text{gr}}) \cdot A_{\text{gr}}(r_{\text{gr}})$. O_{gr} is thus the total surface (= the sum of the surfaces of all grains) contained in 1 m^3 with the unit $\text{m}^2/\text{m}^3 = \text{m}^{-1}$.

The number of molecules desorbed per area and second, i.e. the desorption flux density j_{des} , multiplied with the surface area O_{gr} per m^3 yields the evaporation rate Γ

$$\Gamma = n_{\text{gr}} \cdot A_{\text{gr}} \cdot j_{\text{des}}. \quad (1)$$

The desorption flux density $j_{\text{des}}(T_{\text{gr}})$ depends very sensitively on the grain temperature T_{gr} and increases steeply with increasing temperature. This will be seen to be important.

Photodissociation rates: The density $[\text{H}_2\text{O}]$ of gas phase water increases because of evaporation by Γ and decreases because of photodissociation of water in the first absorption band by $\gamma_1 \cdot [\text{H}_2\text{O}]$. This implies

$$\frac{d}{dt}[\text{H}_2\text{O}] = +\Gamma - \gamma_1 \cdot [\text{H}_2\text{O}], \quad (2)$$

which can be simplified for the stationary case $\frac{d}{dt}[\text{H}_2\text{O}] = 0$ discussed here to:

$$\Gamma = \gamma_1 \cdot [\text{H}_2\text{O}]. \quad (3)$$

Because the first absorption band extends over a large wavelength range from 135 nm to 190 nm the photodissociation rate γ_1 is large and dominated by this band. Other losses, e.g. by photodissociation at shorter wavelength like Lyman α , are neglected up to now. The photodissociation rate γ_1 is determined by the absorption cross section $\sigma_{1\text{st}}$ in the VUV and the spectral photon flux density j_{VUV} emitted by the star, more precisely:

$$\gamma_1 = \int_{1\text{st}} \sigma_{1\text{st}}(\nu) \cdot j_{\text{VUV}}(\nu) d\nu. \quad (4)$$

The spectrum emitted by a new born B/O-star peaks in the VUV region and has a very high luminosity L that may range from $10^4 - 10^6$ solar luminosities (L_0). The short wavelength fraction of the emission below the Lyman α cut-off will be absorbed within the HII region whereas the light beyond the Lyman α cut-off will reach out to the border between the cold interstellar clouds and the HII region. The photodissociation rates vary strongly with the luminosity of the star and the distance between maser and star: for stars with L between 10^4 to 10^6 solar luminosities ($L_0 = 4 \cdot 10^{26}$ W) and a temperature of 25000 K roughly 30% of the luminosity is emitted in the first absorption band. With an average photon energy of 10^{-18} J this yields $1.2 \cdot 10^{48} - 1.2 \cdot 10^{50}$ VUV- photons/s. At a distance of 1000 AU this implies $j_{\text{VUV}} \approx 4 \cdot 10^{18} - 4 \cdot 10^{20} \text{ m}^{-2} \text{ s}^{-1}$ which, with an average absorption cross section of $\sigma_{\text{VUV}} \approx 2 \cdot 10^{-22} \text{ m}^2$ for the first absorption band, yields photodissociation rates between $10^{-3} - 10^{-1} \text{ s}^{-1}$. However at a distance of 200 AU, where the $j = 7/2$ maser may be located, the VUV photon flux will be 25 times larger and vary between $2.5 \cdot 10^{-2}$ and $2.5/\text{s}$. These photodissociation rates are only valid if the VUV photon flux is not attenuated by other species. For the following results the photodissociation rates are varied from $10^{-4}/\text{s}$ (to account for possible attenuation) up to $1/\text{s}$.

Each photodissociation event leads to an OH molecule. Thus the density $[\text{OH}]$ of OH increases due to the photodissociation of water by $\gamma_1[\text{H}_2\text{O}]$. Simultaneously the OH density decreases due to the photodissociation of OH by $\gamma_2[\text{OH}]$.

$$\frac{d}{dt}[\text{OH}] = +\gamma_1[\text{H}_2\text{O}] - \gamma_2[\text{OH}]. \quad (5)$$

Under the stationary condition discussed later on the total OH density is constant ($\frac{d}{dt}[\text{OH}] = 0$) and is then given by (together with Eq. (3)):

$$[\text{OH}] = \frac{\Gamma}{\gamma_2}. \quad (6)$$

Because the absorption cross section of OH is almost identical to that of water (Nee & Lee 1984; Watanabe & Zelikoff 1952; van Dishoeck & Dalgarno 1984) we assume $\gamma_1 = \gamma_2$ and will therefore often use γ for both.

Now we show that the water evaporated from grains attenuates the VUV field not too much. The optical density for the absorption of VUV in the first absorption band of water is given by $\epsilon = [\text{H}_2\text{O}]\sigma_{\text{VUV}}$, where the average absorption cross section is $\sigma_{\text{VUV}} \approx 2 \cdot 10^{-22} \text{ m}^2$. The density of water under stationary conditions is determined according to Eq. (2) by $[\text{H}_2\text{O}] = \Gamma/\gamma$. With a high evaporation rate of $\Gamma = 10^7 \text{ m}^3 \text{ s}^{-1}$ and $\gamma = 10^{-1}/\text{s}$, which we will consider as an extreme case only for the $j = 7/2$ masers, we obtain $[\text{H}_2\text{O}] = 10^8/\text{m}^3$. Even for this upper limit, the optical density is lower than $2 \cdot 10^{-14}/\text{m}$ which implies that the VUV field can penetrate 1000 AU deep into the maser volume. Close to the border of the HII region the attenuation of the VUV by evaporating water is therefore negligible.

2.1. Nascent OH population out of photodissociation of H_2O

Notation of OH quantum states: The OH from the photodissociation of water is formed in different quantum states numbered by the index i . The density of OH in state i is denoted by n_i . We use the labelling of states according to Fig. 1. The four hyperfine states in the ${}^2\Pi_{3/2}$ multiplet states in the $j = 3/2$ OH quantum state are $i = 0 - 3$, where 0, 1 correspond to the lower and 2, 3 to the upper Λ -doublet state. The hyperfine state with the lower F corresponds always to the lower number, i.e., here $i = 0, 2$ for $F = 1$ and $i = 1, 3$ for $F = 2$. The same notation is used for the upper states in ${}^2\Pi_{3/2}$ up to $i = 31$. The states in ${}^2\Pi_{1/2}$ go from $i = 32, \dots, 63$, so that the 8 lowest rotational states with $N \leq 7$ are included in the model. The population of states with larger N is negligible in the photodissociation of water.

The probability for the formation of OH after the photodissociation of water in quantum state i is denoted by f_i with $\sum_i f_i = 1$. For the f_i we use the approach for the Λ -doublet population given in (Andresen 1985) which is roughly valid for the photodissociation of internally cold water. Because a large fraction of the water molecules will relax to lower quantum states before they are photolysed this is probably a good approximation. The nascent OH quantum state distribution is frequency dependent over the first absorption band, in particular for vibrational

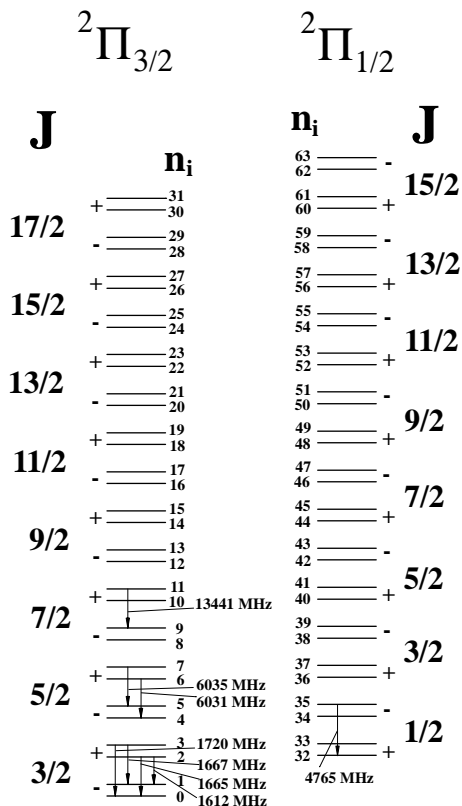


Fig. 1. Diagram of the OH energy levels up to $N = 7$ with the notation used in this paper. The 32 lowest hyperfine states of the $^2\Pi_{3/2}$ ladder are denoted as n_0 to n_{31} and the 32 lowest hyperfine states of the $^2\Pi_{1/2}$ ladder are denoted as n_{32} to n_{63} . The observed maser transitions in W3(OH) are marked with arrows

states. However, the distribution over rotational and Λ -doublet states depends only weakly on frequency. It should be mentioned that the population of the hyperfine states for Λ -doublet states was recently measured to be statistical (Wurps 1997; Thissen et al., submitted 1999).

A warning should be given here because the simplistic picture given above does not hold in detail. The state to state photodissociation yields in some cases even anti-inversion between the Λ -doublets. In addition vibrational excitation can not be neglected. An even more detailed study about the wavelength dependent nascent OH quantum state distribution from single H_2O quantum states is required to improve the present model.

The derived values of f_i are shown in Fig. 3. The nascent population can be calculated from the f_i values. In the stationary case Eqs. (2) and (5) vanish. This gives:

$$n_i = \frac{\Gamma}{\gamma_2} \cdot f_i. \quad (7)$$

The population in each quantum state thus increases with the evaporation rate Γ and decreases with the OH photolysis rate γ_2 .

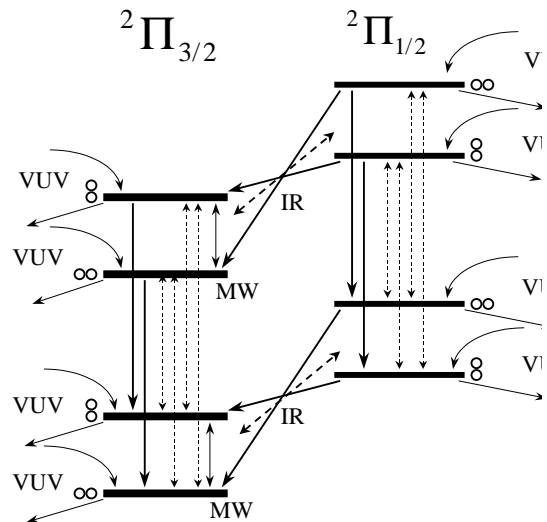


Fig. 2. The Maser Model in a schematic view. The quantum states shown here are the Λ -doublets of OH. Each hyperfine level (not shown here) is fed through photodissociation of water and depopulated via photolysis of OH. In their life time the OH molecules relax to lower states through IR relaxation and stimulated Microwave emission. These transitions are indicated by the solid arrows. The dotted arrows symbolise stimulated emission and absorption of FIR radiation, which is not yet included in the model

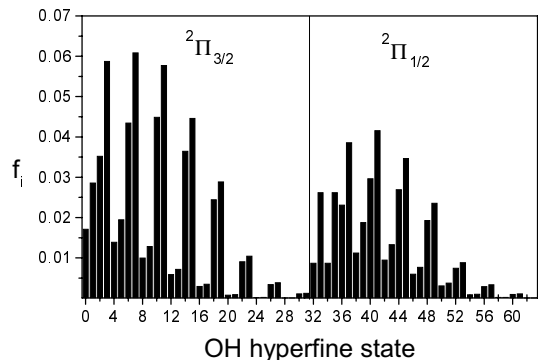


Fig. 3. Nascent OH population out of photodissociation of water as a fraction of the total number of dissociated molecules. In equilibrium with OH photolysis the population is given as $n_i = \frac{\Gamma}{\gamma_2} \cdot f_i$ (Eq. (7))

The reader may be reminded that the total OH density is simply the sum over the OH quantum state populations (compare Eq. (6)).

2.2. OH population including IR relaxation

In this section we will demonstrate that the stationary OH quantum state population resulting from the above model has little to do with the nascent OH quantum state population that results directly from photolysis of water. We will demonstrate that the nascent distribution is considerably modified by an interesting competition between (a)

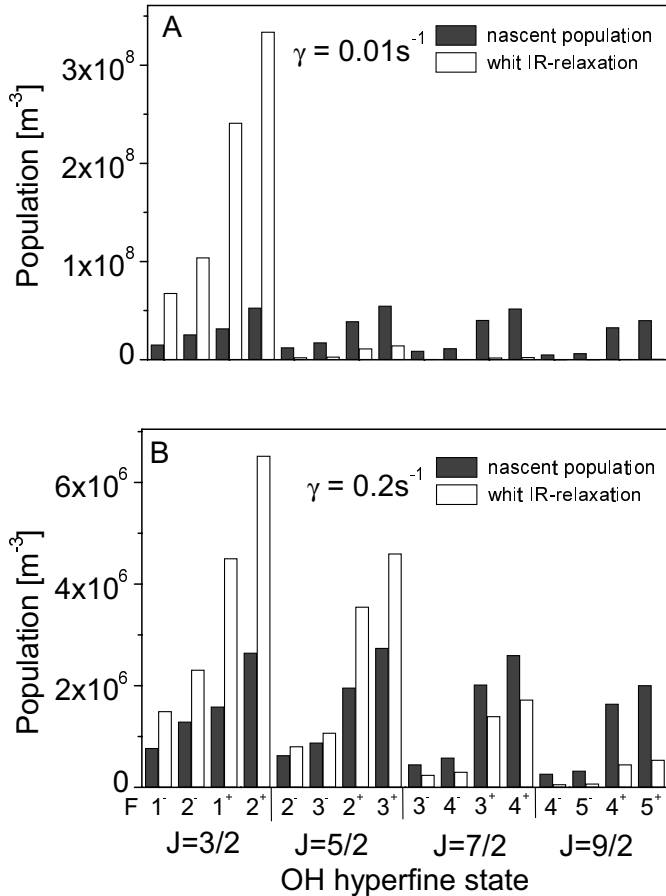


Fig. 4. The effect of IR relaxation on OH quantum state population for two different photodissociation rates at an evaporation rate of $\Gamma = 10^7/\text{m}^3\text{s}$. For small rates γ , as in Fig. 4A, almost all OH molecules relax to the groundstate and yield a very high population of the groundstate. For high photodissociation rates the nascent OH population is much lower because OH is destroyed faster. The distribution over quantum states is less affected. There is still considerable population in the excited states

photodissociation of water (b) subsequent IR relaxation and (c) photodissociation of OH. This competition yields very different OH quantum state distributions for different astrophysical conditions. It will be seen that for the small photodissociation rates that are expected for stars with lower luminosity or further away from a high luminosity star (1) the total OH density is large and (2) the OH quantum state distribution is shifted towards lower states with a very high population in the ground states. In contrast, for the high photodissociation that are expected close to stars with high luminosity (1) the total OH density is much smaller and (2) the OH quantum state distribution is less shifted to lower states and extends further out to higher states.

We will demonstrate that by far the largest population - and therefore the highest gain - is obtained in the ground states for small photodissociation rates. The result

that the highest gain is obtained for low photodissociation rates may be surprising at the first glance but becomes obvious in the following discussion.

The density n_i in quantum state i of OH increases due to photodissociation of water by $f_i\gamma_1[\text{H}_2\text{O}]$ and decreases due to photodissociation of OH by $\gamma_2 n_i$. In addition, the quantum state density decreases because of IR relaxation out of state i to lower states by $\sum_k A_{ik} n_i$, where the sum goes over all final states that can be reached from state i and increases because of IR relaxation from higher states by $\sum_k A_{ki} n_k$. This implies

$$\frac{d}{dt} n_i = +f_i\gamma_1[\text{H}_2\text{O}] - \gamma_2 n_i - \sum_k A_{ik} n_i + \sum_k A_{ki} n_k. \quad (8)$$

The IR relaxation rates are taken from Goorvitch et al. (1992), which includes all transitions possible according to the IR selection rules, e.g. also transitions with $\Delta N = 0, -1, -2$ and $\Delta J = \Delta N - 1$. The data is not resolved according to hyperfine states. The OH is destroyed with the same destruction rate γ_2 in all quantum states.

The equation system is solved numerically. For this we rewrite Eq. (8) as a matrix equation. We define a vector \mathbf{n} by $\mathbf{n} = (n_0, \dots, n_{63})$ representing the density of OH in different quantum states and a vector \mathbf{f} by $\mathbf{f} = (f_0, \dots, f_{63})$ containing the probabilities for the formation of OH in different quantum states as described in Sect. 2.1. We define further a diagonal matrix \mathbf{D} with matrix elements (d_{ij}) with $d_{ij} = \delta_{ij} \sum_k A_{ik}$ which account for the IR relaxation out of state i and a matrix \mathbf{A} with only off diagonal elements A_{ki} which accounts for the IR relaxation into state i from all states k that are above state i and are possible due to the IR selection rules. The matrices contain 64×64 elements. With these definitions we rewrite Eq. (8):

$$\frac{d}{dt} \mathbf{n} = \mathbf{f}\gamma_1[\text{H}_2\text{O}] - \gamma_2 \mathbf{n} - \mathbf{D}\mathbf{n} + \mathbf{A}\mathbf{n} = \mathbf{f}\gamma_1[\text{H}_2\text{O}] + \mathbf{T}(\gamma_2)\mathbf{n} \quad (9)$$

where we introduce the matrix \mathbf{T} by $\mathbf{T}(\gamma_2) = (-\mathbf{E}\gamma_2 - \mathbf{D} + \mathbf{A})$.

For a stationary maser all time derivatives in Eqs. (2, 5, 8, 9, 12, 13) vanish. In particular we have $\frac{d}{dt} \mathbf{n} = 0$ and obtain the quantum state densities from the solution of the matrix Eq. (15)

$$\mathbf{n} = -\mathbf{T}^{-1} \mathbf{f}\gamma_1[\text{H}_2\text{O}] = -\mathbf{T}^{-1} \mathbf{f}\Gamma. \quad (10)$$

For stationary conditions, we have $\Gamma = \gamma_1[\text{H}_2\text{O}]$ according to Eq. (2), which is used in Eq. (10). This implies that the density in every quantum state of OH increases linearly with the evaporation rate Γ by the same amount. The importance of this linearity will be discussed later on.

Figure 4 shows how the OH quantum state populations are affected by the competition between photodissociation and IR relaxation. The population is given here only for the four lowest rotational states of the $^2\Pi_{3/2}$ ladder resolved according to hyperfine structure. An absolute

value of $\Gamma = 10^7/\text{m}^3\text{s}$ is used here for the evaporation rate which determines the total OH density but has no effect on the OH quantum state distribution.

The nascent OH population resulting directly from photodissociation of H_2O is given in both plots (filled bars) to allow an easier comparison with the OH populations resulting from our maser model (open bars) which includes the competition between photodissociation and IR relaxation. The only difference between the two figures is that a $20\times$ smaller photodissociation rate is used in Fig. 4A. The actual value of the photodissociation rates is given in the corresponding figure.

The first and most obvious difference between Figs. 4A and 4B is that more than an order of magnitude larger total OH densities are obtained for the smaller photodissociation rate. The population in Fig. 4A goes up to more than $10^8/\text{m}^3$ whereas it stays at several times $10^6/\text{m}^3$ in Fig. 4B. This somewhat surprising result is easily understood in terms of Eq. (6), which predicts for a $20\times$ larger destruction rate of OH, $20\times$ less total OH. It may be emphasized again that the same evaporation rate is used in both cases. The very large population in the ground state of more than $10^8/\text{m}^3$ leads to large inversion and gain for the ground state masers for low photodissociation rates.

Large differences are also found for the relative distribution among the quantum states. Obviously the nascent distribution differs considerably from that of our maser model. Because IR relaxation transfers population from higher to lower states the distribution obtained from our model is always shifted towards lower states compared to the nascent distribution. This shift is more pronounced for small photodissociation rates because the OH molecules have more time to relax before they are destroyed by photodissociation.

For the small photodissociation rates almost all population is concentrated in the ground state with little population left in excited states. For the high photodissociation rate $\gamma = 0.2/\text{s}$ in Fig. 4B there is still more population in the ground state than in higher states. In comparison to the small photodissociation rate there is relatively more population in the first excited state ($j = 5/2$) and also the $j = 7/2$ state has a non-vanishing population. The excited states are populated more, because at higher dissociation rate (such as $0.2/\text{s}$) the OH molecules have less time to relax before they are destroyed.

It may be interesting to note that the population of the first excited state ($j = 5/2$) is enhanced compared to the nascent population. This is because the IR relaxation out of this state is slower than the IR relaxation into this state. Our results show an enhancement of the population in a given quantum state - relative to the nascent population - as long as the photodissociation rate γ exceeds the IR relaxation rate $A_{\text{IR}}(j)$ of this particular rotational state (e.g. $A_{\text{IR}}(j = 5/2) = 0.136/\text{s}$, $A_{\text{IR}}(j = 7/2) = 0.514/\text{s}$, $A_{\text{IR}}(j = 9/2) = 1.25/\text{s}$).

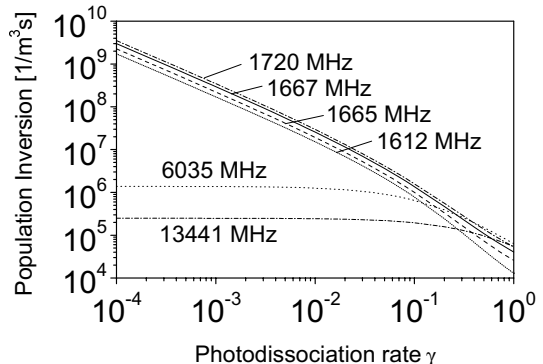


Fig. 5. Population inversion ($n_u - n_l$) for the masers observed in W3(OH) calculated from the present model. The evaporation rate was chosen to be $\Gamma = 9 \cdot 10^6/\text{m}^3\text{s}$. The population and the population inversion increase strongly with decreasing the dissociation rates. This is due to the fast relaxation from excited states. In contrast the inversions in the excited states are nearly constant over a large range of dissociation rates. For the inversion in the excited states there is a sharp bend off at the position when the dissociation rate becomes as large as the IR relaxation rate for this state ($A_{\text{IR}}(j = 5/2) = 0.136 \text{ s}^{-1}$, $A_{\text{IR}}(j = 7/2) = 0.514 \text{ s}^{-1}$)

In order to evaluate the influence of the photodissociation rate in a more detailed way the population inversion for some important OH maser transitions is plotted in Fig. 5. The population inversion PI_{ul} is defined as the difference between the population of the upper level (n_u) and the population of the lower level (n_l):

$$PI_{ul} = n_u - n_l. \quad (11)$$

In Fig. 5 the population inversion is plotted as a function of the photodissociation rate γ . The evaporation rate is chosen here to be $\Gamma = 9 \cdot 10^6/\text{m}^3\text{s}$.

The inversion in the excited states behaves in a very different manner than the inversion in the ground state. Whereas the inversion in the ground state increases dramatically with decreasing dissociation rates it remains almost constant for the excited states for small dissociation rates and drops off only at larger dissociation rates. This effect was already discussed above but becomes more obvious here. This effect is understood in terms of the different losses out of the ground and excited states: losses due to IR relaxation occur only out of the excited states whereas there is no such loss out of the ground state. Because the only loss in the ground state results from destruction of OH by photodissociation these losses decrease with decreasing dissociation rate.

For the excited states the loss rate is dominated by the losses due to IR relaxation, which is independent of γ . This leads to an almost constant population inversion for low dissociation rates, which is, however, much smaller than in the ground state. Only at dissociation rates higher than $0.1/\text{s}$ the losses due to photodissociation become comparable to the losses due to the IR relaxation. This causes the

population and therefore the population inversion to go down. This bend-off is weaker for the higher excited states than for the lower lying excited states and the ground state.

It may be interesting to note that for higher γ 's ($> 0.3/\text{s}$) the population inversion becomes higher in the excited states than for the ground states.

2.3. Collisional effects

Up to now we neglected collisional effects. Here we show why. To estimate the relative importance of collisions versus photodissociation, the OH collisional probability p_c (= probability for an OH collision per s) is compared with the OH photodissociation rates γ_2 . We consider only collisions with H_2 because this is expected to be the dominant species in the interstellar medium. This implies $p_c = [\text{OH}]^{-1} \cdot \frac{d}{dt}[\text{OH}] = k[\text{H}_2]$. An order of magnitude estimate for the rate constant k for inelastic OH– H_2 collisions is obtained from $k = \sigma_c v$ with the cross section σ_c for inelastic collisions and the velocity v . For a typical cross section of $\sigma_c \approx 10^{-15} \text{ cm}^2 = 10^{-19} \text{ m}^2$ and the nascent OH velocity from the photodissociation of water $v = 1.3 \cdot 10^3 \text{ m/s}$ we obtain $k \approx 1.3 \cdot 10^{-16} \text{ m}^3/\text{s}$.

The H_2 densities are not expected to exceed 10^{14} m^{-3} . This yields a collisional probability $p_c = k[\text{H}_2] \approx 10^{-2}/\text{s}$. According to the discussion above, the photodissociation rates are expected to vary between $10^{-3}/\text{s}$ and $1/\text{s}$. This implies that collisions will affect the OH quantum state densities only for small photodissociation rates.

Because the IR relaxation from excited states is fast, the excited state OH masers have to be pumped fast to compete with IR relaxation. We assume that at least for the case of the 13441 MHz ($j = 7/2$) with relaxation rates of 0.5 s^{-1} collisions can be neglected safely. Even effects like FIR pumping will play a minor role so that the present model is expected to hold better for the excited state masers.

2.4. Stimulated emission, gain and amplification

In this section we determined gain and amplification resulting from our model for different maser transitions under different astrophysical conditions. As a first step we operate only in the limit of the exponential small signal gain but give estimates for the onset of saturation.

If the lower and upper maser level are denoted by l and u , respectively, we obtain:

$$\frac{d}{dt}n_l = +f_i\gamma_1[\text{H}_2\text{O}] - \gamma_2n_l - \sum_k A_{lk}n_l + S_{ul}n_l - S_{ul}n_u \quad (12)$$

$$\frac{d}{dt}n_u = +f_i\gamma_1[\text{H}_2\text{O}] - \gamma_2n_u - \sum_k A_{uk}n_u - S_{ul}n_u + S_{ul}n_l \quad (13)$$

Table 1. Frequency and Einstein A -coefficients according to Destombes et al. (1977) and the calculated stimulation cross section (see Eq. (17))

J	Transition	ν [MHz]	A_{ij} [$10^{-10}/\text{s}$]	σ_{ij}^0 [10^{-18} m^2]	I_{sat} [$10^{15} \frac{\text{Photons}}{\text{m}^2\text{s}}$]
${}^2\Pi_{3/2}$ ($j = 3/2$)	$1^+ \rightarrow 2^-$	1612.2	0.1302	1.489	6.71
	$1^+ \rightarrow 1^-$	1665.4	0.7177	7.448	1.34
	$2^+ \rightarrow 2^-$	1667.4	0.7778	8.043	1.24
	$2^+ \rightarrow 1^-$	1720.5	0.0949	0.894	11.18
${}^2\Pi_{3/2}$ ($j = 5/2$)	$2^+ \rightarrow 3^-$	6016.7	1.098	0.242	41.32
	$2^+ \rightarrow 2^-$	6030.7	15.48	3.382	2.95
	$3^+ \rightarrow 3^-$	6035.1	15.83	3.450	2.89
	$3^+ \rightarrow 2^-$	6049.1	0.797	0.172	58.14
${}^2\Pi_{3/2}$ ($j = 7/2$)	$4^+ \rightarrow 3^-$	13433.9	2.665	0.053	188.67
	$3^+ \rightarrow 3^-$	13434.6	92.52	1.828	5.47
	$4^+ \rightarrow 4^-$	13441.4	93.43	1.843	5.42
	$4^+ \rightarrow 3^-$	13442.1	3.433	0.068	147.06
${}^2\Pi_{1/2}$ ($j = 1/2$)	$0^- \rightarrow 1^+$	4660.2	10.92	5.169	1.93
	$1^- \rightarrow 1^+$	4750.6	7.713	3.447	2.90
	$1^- \rightarrow 0^+$	4765.5	3.893	1.724	5.80

S_{ul} is the stimulation rate. The stimulation rate is related to the maser photon flux j_m (photons per m^2 and s) and the cross section σ_{ul} for stimulated emission by

$$S_{ul} = \sigma_{ul}j_m. \quad (14)$$

The frequency integrated cross sections $\int \sigma_{ul}(\nu)d\nu$ for the stimulated emission are obtained from the Einstein A -coefficients from Destombes et al. (1977) via

$$\int \sigma_{ul}(\nu)d\nu = \frac{A_{ul}c^2}{8\pi\nu^3}. \quad (15)$$

The line width for the OH resulting from the photodissociation of water is given by the nascent velocity v_{OH} according to the Doppler effect by

$$\Delta\nu = \frac{2 \cdot v_{\text{OH}}}{c}. \quad (16)$$

With the nascent velocity of OH we have $v_{\text{OH}} \approx 1.3 \cdot 10^3 \text{ m/s}$ and therefore $\Delta\nu \approx 10^{-5}\nu$. If we introduce the peak absorption cross section σ_{ul}^0 by $\int \sigma_{ul}(\nu)d\nu = \sigma_{ul}^0 d\nu = \sigma_{ul}^0 10^{-5} \cdot \nu$ we obtain

$$\sigma_{ul}^0 = \frac{A_{ul} 10^5 \cdot c^2}{8\pi\nu^3}. \quad (17)$$

Equation (17) is used to calculate the (peak) cross section for stimulated emission for all observed maser frequencies. Table 1 gives the frequencies, Einstein A coefficients, the calculated σ_{ul}^0 and the microwave flux I_{sat} for the onset of saturation for all maser transitions. Here the onset of saturation is defined as

$$I_{\text{sat}} \cdot \sigma_{ul} = 5\%, \quad (18)$$

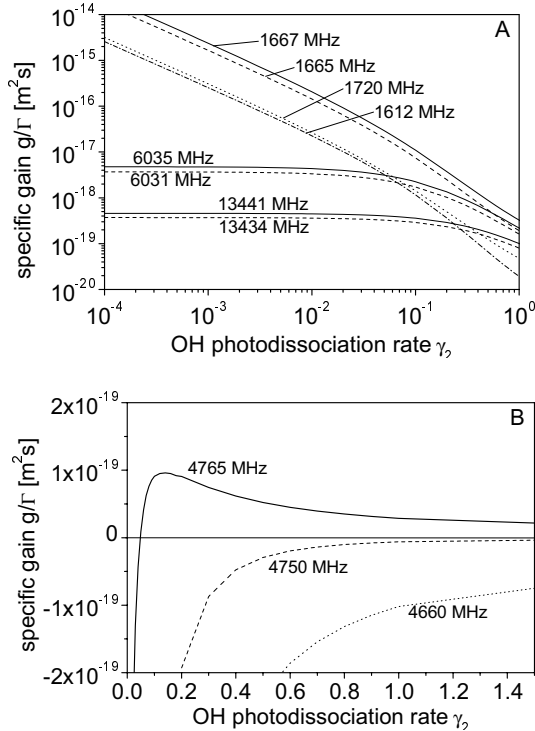


Fig. 6. The specific gain calculated from our model for all maser transitions observed in W3(OH). The absolute gain can be derived by multiplying the specific gain with the evaporation rate Γ

which means: The change in population due to the stimulated emission exceed 5 per cent of the population.

For the amplification of the photon flux along some propagation direction z we use the peak cross section for stimulated emission and obtain:

$$\frac{d}{dz} j_m = \sigma_{ul}^0 (n_u - n_l) j_m. \quad (19)$$

This implies a small signal gain

$$g = \sigma_{ul}^0 (n_u - n_l). \quad (20)$$

As seen in Sects. 2.1 and 2.2 the OH population is proportional to the evaporation rate Γ . Now we introduce a quantity called “specific gain” g_s , which is defined as

$$g_s = \frac{g}{\Gamma} = \frac{\sigma_{ul}^0 (n_u - n_l)}{\Gamma}. \quad (21)$$

The specific gain is the gain obtained if one water molecule is evaporated in 1 m^3 per second. The specific gain is used here because it is independent of the evaporation rate and describes the physics for the competition between photodissociation and IR relaxation. g_s is a characteristic feature of the proposed pumping scheme. The specific gain for the OH maser transitions observed in W3(OH) is displayed in Fig. 6.

Figure 6A shows the specific gain for the maser transitions in the $^2\Pi_{3/2}$ ladder as a function of the

photodissociation rate γ . In general, the results for the specific gain are similar to those for the population inversion that was shown in Fig. 5. This is not surprising because, apart from the evaporation rate, the only important difference between specific gain and population inversion is the different cross section for stimulated emission (compare Eq. (20)). The comparison between Figs. 5 and 6 thus shows the effects resulting from the different cross sections for stimulated emission. The general agreement in features, like increase of the specific gain in the ground state with decreasing γ or the bend-over for the excited state at larger dissociation rates are therefore easily understood.

A large difference appears between specific gain and inversion for the main and satellite lines in the ground state. The specific gain for the 1612 MHz and 1720 MHz masers is much smaller than for the 1667 MHz and 1665 MHz masers although the inversion is similar. This is a result of the roughly $10\times$ smaller stimulation cross section σ_{ul}^0 for the satellite lines compared to the main lines.

For the excited states the specific gain is again almost constant over a wide range of γ 's and decreases when the photodissociation rate becomes as large as the IR relaxation rate. Because the stimulation rates are smaller for the excited states the specific gain - in contrast to the population inversion - is always smaller in the excited states than for the ground state main line transitions.

This seems to propose that ground state masers should dominate excited state masers even at high dissociation rates. Such conclusions cannot be drawn. First, it is not clear how the much larger spontaneous emission rates in the excited states compared to the ground state affect the appearance of a given maser transition.

Second, if the dissociation rates become larger than the IR relaxation rates, the population distribution for both the ground and excited states approaches the nascent population from direct photolysis. The nascent inversion in the ground state, however, depends strongly on the population of quantum states in the parent water molecule (Häusler et al. 1987). Photodissociation of the rotational ground state of water even yields anti-inversion for the ground state transitions in OH. For small dissociation rates this effect is less important because the high nascent inversion in the high lying rotational states is transferred to the ground state. This is because the IR relaxation conserves the inversion. Consequently the model given above is too simple for the ground state at large dissociation rates. A closer look at this problem reveals that for high γ 's the picture will change but remain more or less constant for low γ 's, because the population inversion is then more determined by IR relaxation from highly inverted upper rotational states.

Figure 6B shows the specific gain for the three transitions of the $^2\Pi_{1/2}(j = 1/2)$ state. Photodissociation of H_2O yields anti-inversion between all Λ -doublets of the $^2\Pi_{1/2}$ multiplet and therefore yields a “negative

specific gain” as seen for the 4750 MHz and the 4660 MHz transitions in Fig. 6B. For the 4765 MHz transition, however, a different behavior is observed. Here the specific gain is still negative for small dissociation rates below 0.05/s as expected. However, for $\gamma > 0.05/s$ g_s the specific gain becomes positive with a maximum of $g_s \approx 10^{-19} \text{ m}^2 \text{ s}$ at $\gamma \approx 0.1/s$. Nevertheless the specific gain stays small and it may be hard to explain this maser without additional mechanisms like FIR pumping.

The gain g is obtained from the specific gain g_s by multiplication with Γ . It will be seen below that Γ can vary strongly with the astrophysical conditions and depends sensitively on the density, sizes and temperatures of the grains. This implies in turn a large variation of maser phenomena with different astrophysical conditions.

The calculations given below neglect saturation effects which implies exponential growth of the maser intensity and yields for an amplification factor V_m

$$V_m = \frac{j_m}{j_{m_{in}}} e^{gz} \quad (22)$$

where $j_{m_{in}}$ is the incoming maser photon flux density and z is the length of the maser volume. Although the formalism presented above includes saturation effects these are excluded here and postponed to a future paper.

Some examples: Now we give some specific examples for the gain g and the amplification factors V_m obtained for different maser transitions at different evaporation rates.

In Fig. 6 it can be seen that the specific gain in the $j = 3/2$ maser can become very large, in particular for dissociation rates lower than 0.01 s^{-1} . Under these circumstances population and inversion are accumulated in the ground state due to IR-relaxation with little OH destroyed by photodissociation. Note that the nascent inversion in the ground state is lower than the inversion after relaxation.

This is illustrated by an example with a photodissociation rate of $\gamma_1 \approx 0.01 \text{ s}^{-1}$, where we obtain a specific gain of $2 \cdot 10^{-16} \text{ m}^2 \text{ s}$ for the 1667 MHz maser. A moderate evaporation rate of $\Gamma \approx 3 \cdot 10^3 \text{ m}^{-3} \text{ s}^{-1}$ yields a gain of $6 \cdot 10^{-13} \text{ m}^{-1}$, which implies under the assumption of exponential growth an amplification of $V_m = 10^6$ for a tube length of roughly 150 AU. For the 6035 MHz maser the specific gain is $g_s \approx 5 \cdot 10^{-18} \text{ m}^{-1}$ for γ_1 below 0.1/s. Nevertheless, a gain of $\approx 2.5 \cdot 10^{-12} \text{ m}^{-1}$ can be obtained, with a much higher evaporation rate of $\Gamma = 5 \cdot 10^5 \text{ s}^{-1}$, however. In this case an amplification of 10^6 is obtained with a tube length of roughly 60 AU.

For the 13.44 GHz maser the specific gain is even smaller. In the range of low photodissociation rates we have $g_s \approx 3.5 \cdot 10^{-19} \text{ m}^2 \text{ s}$. To explain the gain of $\gamma = 2 - 3 \cdot 10^{-12} \text{ m}^{-1}$, suggested by Baudry & Diamond (1998) for the single bright maser spot in W3(OH), an even higher evaporation rate of $\Gamma \approx 9 \cdot 10^6 \text{ m}^{-3} \text{ s}^{-1}$ is required. This

gain yields an amplification of $V_m = 10^3$ for a tube length of 15 AU. It should be mentioned that there is a general background of 20 mJy at the maser frequency from all over the region of this maser. The amplification of this background by $V_m = 10^3$ yields exactly the 20 Jy observed for the single bright maser spot.

For the 4765 MHz maser in ${}^2\Pi_{1/2}(j = 1/2)$ state gain is obtained only for photodissociation rates above 0.05/s. The maximum specific gain is obtained for $\gamma \approx 0.1 \text{ s}^{-1}$ and is there around $g_s = 1 \cdot 10^{-19} \text{ m}^2 \text{ s}$, the smallest specific gain from all observed masers. Even with $\Gamma = 10^7 \text{ m}^{-3} \text{ s}^{-1}$ we obtain a gain of only 10^{-12} m^{-1} and require a tube length of 50 AU for an amplification of 1000. This maser operates according to the present model only if the photodissociation and the evaporation rates are high.

To summarize the results from our gain considerations, we state that over a wide range of γ 's specific gain is obtained for all observed maser transitions that appear in regions of star formation. In contrast to the specific gain, the gain itself depends strongly upon the evaporation rates. For the same evaporation rate the relative gain between different states is determined by the relative specific gains. The specific gain for the excited state masers in ${}^2\Pi_{3/2}$ is much smaller than for the ground state masers. Small specific gain is obtained also for the 4765 MHz maser, however, only for γ above 0.05/s. Much smaller specific gain is also obtained between states higher than $j = 7/2$ in ${}^2\Pi_{3/2}$ where no masing is observed. However, the gain is so small for these states that masing is not expected from the present maser model, in agreement with observations.

For all states in ${}^2\Pi_{3/2}$ the gain for the F state with higher multiplicity dominates the gain with lower multiplicity. This predicts a preference for hyperfine transitions in the sense that the transition belonging to the larger F -value should be stronger. For the ground state masers the gain for the main lines dominates that for satellite lines. Because the specific gain can become very high in the ground state the satellite lines are also expected to yield maser radiation with a slight preference for the 1720 MHz transition.

2.5. Spontaneous emission and “self oscillation”

Here we discuss whether spontaneous emission from a tubular volume with cross sectional area \mathcal{A} and length l can start the maser even without external background emission from e.g. grains. We use the quantum state populations given in Sect. 2.2. We consider an infinitesimal element dz along the maser's propagation direction z which has a volume $dV = \mathcal{A}dz$ with a density n_u in the upper maser level. The number of spontaneous emission events from this volume is $A_{ul}n_u\mathcal{A}dz$ per second. The fraction $\Delta\Omega/4\pi = \mathcal{A}/4\pi l^2$ of these spontaneous photons passes through the exit area of the maser tube. Only these spontaneous photons will propagate through the inverted maser volume, will be amplified on this path and

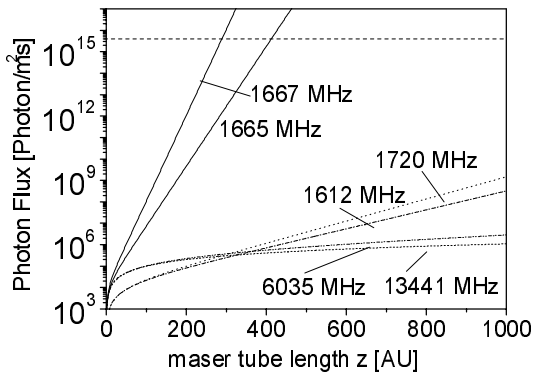


Fig. 7. Maser output as a function of the maser tube length as calculated from our model for $\Gamma = 3 \cdot 10^3 / \text{m}^3 \text{ s}$ and $\gamma = 0.01 \text{ s}^{-1}$ assumed for a distance of 1000 AU from the central star. It becomes clear that only the ground state maser can operate under these conditions. The excited state masers require higher evaporation rates and photodissociation rates. The dashed line marks the onset of saturation for the ground state main line transitions

contribute to the maser emission observed on earth. The maser photon flux density that exits the front area \mathcal{A} of the maser tube is then $A_{ul}n_u\mathcal{A}dz(\Delta\Omega/4\pi)/\mathcal{A}$. The maser flux density will give rise also to the stimulated emission $j(z)\sigma_{ul}(n_u - n_l)\mathcal{A}dz$ in the volume $\mathcal{A}dz$. The increase dj of the maser flux density results therefore not only from the spontaneous emission $A_{ul}n_u dz(\Delta\Omega/4\pi)$ but also from the stimulated emission $j(z)\sigma_{ul}(n_u - n_l)\mathcal{A}dz$ which implies

$$\frac{dj}{dz} = j(z)\sigma_{ul}(n_u - n_l) + \frac{\Delta\Omega}{4\pi} \cdot A_{ul}n_u. \quad (23)$$

With the gain $g = \sigma_{ul}(n_u - n_l) = g_s\Gamma$, this can be solved as long as the maser is not saturated by

$$j(z) = \frac{\Delta\Omega}{4\pi} \frac{A_{ul}n_u}{g} (e^{g_s\Gamma \cdot z} - 1). \quad (24)$$

Figure 7 shows results for the maser photon flux density obtained from spontaneous and stimulated emission for the maser transitions appearing in regions of star formation as a function of the maser tube length. The evaporation rate is taken to be $\Gamma = 3 \cdot 10^3 / \text{m}^3 \text{ s}$ and the photodissociation rate is $\gamma = 0.01 / \text{s}$ as assumed for a distance of ≈ 1000 AU from the central star. Under these condition only the ground state masers will start with spontaneous emission. In the present model only exponential growth and no saturation effect are encountered (see Eq. (24)). The emitted photon flux is largest for the main line ground state masers because their specific gains are largest at this particular dissociation rate. The 1667 MHz maser reaches the onset of saturation (see Table 1) at a tube length of ≈ 250 AU.

In contrast, the ground state satellite line masers and the excited state maser show a much smaller growth under these conditions that are chosen to explain the main line ground state masers. This results from their much smaller

specific gain which in turn comes from the small evaporation rate of only $\Gamma = 3 \cdot 10^3 / \text{m}^3 \text{ s}$. This implies the main line ground state masers will work even far away from the star, whereas the excited state masers will not operate there. According to the discussion below much higher evaporation rates may be expected closer to the star. There the specific gains of the different maser transitions becomes more similar at the expected higher dissociation rates (see Fig. 6). The competition between the masers under these conditions (closer to the star) have not been investigated yet.

Nevertheless the results show that with reasonable tube length the ground state maser may start with spontaneous emission without any amplification of background radiation from the surrounding dust shell. At a given maser tube length the output becomes higher with such additional microwave background radiation.

3. Evaporation rates and life time of masers

According to the present maser model, all masers observed at new born stars have gain and can yield maser radiation by photodissociation of the gaseous water evaporated from grains in the presence of VUV radiation. Because the gain increases linearly with the evaporation rate, the present maser model can yield any gain with sufficiently high evaporation rates. For the gains presented above, we simply postulated evaporation rates ranging from $\Gamma = 10^3 - 10^7 \text{ m}^{-3} \text{ s}^{-1}$ without any critical discussion of whether such rates are possible at all. In this section we try to establish order of magnitude estimates for the evaporation rates for the special astrophysical conditions at the border between a HII region and the surrounding cloud of grains.

It should be mentioned that the evaporation problem is closely related to an often discussed criticism of the photodissociation pump mechanism. The evaporation rate is responsible for the replacement of the large amount of gaseous water that is destroyed by photodissociation. Only with sufficient evaporation going on for an extended time the masers can operate without turning off. In the present stationary maser model the evaporation rate Γ equals the number of water molecules destroyed per m^3 and second (see Eq. (2)). An evaporation rate of $\approx 10^7 \text{ m}^{-3} \text{ s}^{-1}$ is necessary if e.g. 10^7 water molecules are destroyed per m^3 and second! The question is whether such high evaporation rates are possible at all. The stationary maser model given here implies a highly dynamical equilibrium between evaporation and destruction in which the densities of OH and H_2O adjust to the given photodissociation rates. In this suggested mechanism the evaporated water is converted to translationally hot hydrogen atoms and relatively low oxygen atoms by the VUV radiation from the central star and heats the environment in areas where water is evaporated (“photolytic heating”).

The region around the star that is exposed to the direct heat- and VUV- flux from the star will reach out only to a region where small grains are present in high abundance. With a grain density of $n_{\text{gr}} \approx 1 \text{ m}^{-3}$ for $1 \mu\text{m}$ grains, which is considered to be typical for cold interstellar clouds, an optical density of $\epsilon = n_{\text{gr}}\sigma_{\text{gr}} \approx 3 \cdot 10^{-12} \text{ m}^{-1}$ is obtained. This implies that the radiation will be attenuated to $1/e$ along a distance of only $\approx 2 \text{ AU}$. This thin layer of a few AU thickness blocks the direct radiation. Although the radiation will diffuse further out, it is expected that there will be no VUV beyond that border. We will use the term “small grain border” for this thin layer below.

The small grains at this border are exposed to the direct heat flux from the star and will be evaporated with time leading to a growth of the HII region. The time until complete evaporation increases with the size of the grains. If the small $1 \mu\text{m}$ grains are already completely evaporated larger grains will remain at the inner side of the small grain border. Because their evaporation takes a longer time they will be a source of gas phase water molecules which are exposed to the VUV field from the central star. If we assume in addition that the grains move with their gravitational velocity towards the star large grains will penetrate deeper into the HII region than small grains. Because the optical density of the remaining large grains is much lower than that for the small grains at the border they are exposed to the direct heat- and VUV- flux from the star. This increases with decreasing distance to the star. Consequently evaporation and photolysis of water takes place simultaneously in this regions and yields the astrophysical situation where the present maser model applies. Below we will discuss the processes that occur to the larger grains at the inner side of the small gain border in more detail.

For a single grain the evaporation is determined mainly by its surface area and temperature. The surface temperature depends on the heat transfer from and to the surface. The heat transferred to the surface results from the direct heat flux from the star and from collisions with the surrounding gas, including e.g. the heat resulting from the adsorption of water or atoms that are generated by photolytic heating. The heat losses result from black body radiation, heat conduction to the bulk and evaporative cooling by desorption.

The evaporation of grains is extremely difficult to predict quantitatively because it depends on too many and mostly unknown parameters. Features like porosity or chemical composition of the surface strongly affect surface area and temperature leading to large variations in the evaporation rate. This problem is well known from comets (e.g. Combi et al. 1998; Schultz et al. 1992) where the identical problem is encountered. The astrophysical problem of the evaporation from grains near new born stars may also be compared with the evaporation of droplets in spray combustion where large difficulties are encountered in a quantitative treatment despite massive experimental and theoretical efforts. Because it is impossible to de-

rive quantitative evaporation rates we restrict ourselves to a qualitative discussion of evaporation immediately from the analogy with spray combustion. The large droplets survive longer than small droplets in spray evaporation and penetrate deeper into the gas.

There are nevertheless some important qualitative conclusions which can be drawn. Here larger grains live longer when they are exposed to the direct heat flux from the star and penetrate the HII region deeper than the small grains. Closer to the star they are exposed to an increasing heat flux, acquire larger temperatures and may yield rather high evaporation rates in the presence of intense VUV radiation there.

To determine the evaporation rate ($\Gamma = O_{\text{gr}}j_{\text{des}}$) both the desorption flux density j_{des} and the surface area of all grains in m^3 maser volume have to be known. The desorption flux density is closely related to the vapour pressure of ice. Under thermal equilibrium conditions the same number of water molecules are adsorbed and desorbed on the surface, i.e., the desorption flux density j_{des} equals the adsorption flux density j_{ads} . We approximate the adsorption flux density by $j_{\text{ads}} = 1/6 nv$ with the gas phase density $n = p/kT$ and velocity $v = (2kT/m)^{0.5}$. This implies $j_{\text{des}} = (18mkT)^{-0.5} p$ with the vapour pressure p of ice. For the vapour pressure p of ice we use the well known standard expression $p = A \exp(-B/T)$ (Handb. of Chem. Phys.). With $\alpha = (18mk)^{-0.5}A$ and $\beta = B$ this yields

$$j_{\text{des}} = \alpha \sqrt{T} e^{-\beta/T}. \quad (25)$$

With $\beta = 5.11 \cdot 10^3 \text{ K}$ and $\alpha = 3.32 \cdot 10^{34} \frac{1}{\text{sm}^2 \sqrt{\text{K}}}$ this expression yields the correct vapour pressure of water at 100°C and 0°C . The desorption flux density thus depends only on the surface temperature and increases exponentially with increasing temperature. For example, j_{des} increases from $j_{\text{des}} \approx 10^{15} \text{ m}^{-2} \text{ s}^{-1}$ at $T = 120 \text{ K}$ over $2 \cdot 10^{22} \text{ m}^{-2} \text{ s}^{-1}$ at 200 K to $j_{\text{des}} \approx 2.8 \cdot 10^{24} \text{ m}^{-2} \text{ s}^{-1}$ at 250 K . Nevertheless, Eq. (25) is only used to obtain order of magnitude estimates for j_{des} .

The evaporating grains have a finite life time that is determined by their surface temperature and their mass. In this qualitative discussion we neglect adsorption which would yield an even longer life time. Because $j_{\text{des}}A_{\text{gr}}dt$ is the number dZ of water molecules desorbing from the grain in the time dt , we have $dZ/dt = j_{\text{des}}A_{\text{gr}}$. With the density $\kappa \approx 3 \cdot 10^{28} \text{ m}^{-3}$ of ice, the total number of water molecules on a grain is $Z = \kappa V_{\text{gr}} = \kappa \frac{4}{3} \pi r_{\text{gr}}^3$ under the assumption of spherical grains. Therefore $dZ/dt = d/dt(\kappa \frac{4}{3} \pi r_{\text{gr}}^3) = \kappa \frac{4}{3} \pi r_{\text{gr}}^2 dr_{\text{gr}}/dt$ which yields $\kappa \frac{4}{3} \pi r_{\text{gr}}^2 dr_{\text{gr}}/dt = j_{\text{des}}A_{\text{gr}} = j_{\text{des}}4\pi r_{\text{gr}}^2$. This simple model yields a decrease of the grain radius with time that is independent of the grain radius:

$$\frac{dr_{\text{gr}}}{dt} = \frac{3}{\kappa} j_{\text{des}}. \quad (26)$$

The time t_1 required to desorb all water molecules off the grain, i.e., the life time of a grain is

$$t_1 = \frac{\kappa}{3j_{\text{des}}r_{\text{gr}}} . \quad (27)$$

If r_{gr} is measured in μm and t_1 is given in years we obtain, for example, at a constant grain temperature of $T = 120$ K and the desorption flux $j_{\text{des}} \approx 10^{15} \text{ m}^{-2} \text{ s}^{-1}$ corresponding to this temperature a grain life time of

$$t_1 = 0.317 \cdot r_{\text{gr}} . \quad (28)$$

The life of a grain depends linearly on its radius. Grains with $100 \mu\text{m}$ radius last ≈ 30 years, grains with $10 \mu\text{m}$ for ≈ 3 years and $1 \mu\text{m}$ only for ≈ 0.3 years at 120 K. Large “grains” with radii of 10 km, like comets, will live 10^8 times longer. As mentioned above, we assume that the grains move towards the central star with their gravitational velocity and will travel $\approx 1 \text{ AU/year}$ for a velocity of e.g. $v \approx 5 \cdot 10^3 \text{ m/s}$. This implies that grains of increasing sizes will penetrate deeper and deeper beyond the border of the HII region. $100 \mu\text{m}$ ($10 \mu\text{m}$, $1 \mu\text{m}$) grains at $T = 120$ K will travel roughly 30 AU (3 AU, 0.3 AU) towards the star before they are completely evaporated.

It is an obvious but important result that small grains are evaporated much faster than large grains and that large grains penetrate deeper. The same effect occurs as mentioned above in the evaporating sprays in Diesel engines where big droplets live much longer than small droplets and penetrate much deeper into the hot gas. This is well known to create one of the most important problems in Diesel combustion, i.e., soot formation which is avoided in modern engines today by the generation of finer droplets.

The importance of the above consideration should be stressed again: The larger water carrying grains penetrate the HII region and are evaporated in a region where they are exposed to the VUV radiation field. Large grains, like comets, may penetrate very deep in the HII region where the heat flux goes up and massive evaporation of water molecules sets in and intense VUV radiation fields are present for sure. This yields the astrophysical situation in which grains are exposed to the heat- and VUV- flux from the star, the situation in which our maser model applies.

Groundstate Masers: We will now try to explain the ground state masers based on the astrophysical conditions met at the border of the HII region in a layer which may be a few tenths of AU thick, at the inner side of the small grain border where relatively small grains of $10 - 100 \mu\text{m}$ are still present and evaporate water. Then we will try to explain the excited state masers by the evaporation from much larger grains that penetrate deeper and may thus reach much higher temperatures there. Because these larger grains have finite life time the excited state masers should be transient phenomena.

First we treat the region close to the border of the small grain region. We calculate the grain density required for the evaporation rate of $\Gamma = 3 \cdot 10^3 \text{ m}^{-3} \text{ s}^{-1}$ that was used above to discuss $j = 3/2$ masers. We assume a temperature of 120 K and obtain, according to Eq. (1), this rate Γ with $O_{\text{gr}} = n_{\text{gr}}A_{\text{gr}} = 3 \cdot 10^{-12} \text{ m}^2/\text{m}^3$. This surface area (per m^3 maser volume) originates from a grain size distribution that is not known. If we assume spherical $10 \mu\text{m}$ ($100 \mu\text{m}$) grains the required surface of area $3 \cdot 10^{-12} \text{ m}^2/\text{m}^3$ is obtained with a grain density of $n_{\text{gr}} \approx 24 \cdot 10^{-3} \text{ m}^{-3}$ ($24 \cdot 10^{-6} \text{ m}^{-3}$). Much lower grain densities would result for highly porous grains. If we compare these grain densities to the often used grain density of $1/\text{m}^3$ for $1 \mu\text{m}$ grain in cold clouds, this does not seem to be too exotic.

This implies that a gain of $g = 10^{-12} \text{ m}^{-1}$ is obtained for the $j = 3/2$ maser with e.g. a moderate grain density of only 24 grains with $100 \mu\text{m}$ radius in a volume of 10^6 m^3 . These $100 \mu\text{m}$ grains would live at $T = 120$ K for roughly 30 years and penetrate the HII region 30 AU in this time. The continuous flow of grains towards the star could thus replace the grains that are evaporated or the masers may simply move outwards with the expansion velocity of the HII region. This mechanism implies that the ground state masers can last as long as the cloud surrounding the HII region is not expanded so much that the evaporation and photodissociation rate become too small.

According to this picture the ground state OH masers could result from the evaporation of grains e.g. in the range of $10 - 100 \mu\text{m}$ that lie in the circumstellar shell at the inner side of the small grain border. In this situation large maser tube lengths of several 100 AUs are possible tangentially to the border, i.e. large gain lengths are possible which in turn can yield intense ground state masers.

Excited State Masers: The long lived larger grains suffer a different fate. On their continuing way towards the star they penetrate the HII region deeper and are exposed to an increasingly higher heat flux from the star. Due to the increasing heat flux with decreasing distance the surface temperature of the large grains will rise and the desorption flux as well as the evaporation rate will increase fast. Because the small grains are already completely evaporated deep inside the HII region the large grains there are exposed to the full direct heat and VUV flux. Then both water and OH are photolyzed efficiently to give H and O atoms. Because an energy of a few eV per photolyzed molecule goes to the gas surrounding the grain the gas heats up even more. This “photolytic heating” is well known for the comets approaching the sun. Consequently there is increasingly massive evaporation if a large grain approaches the star. Once the grain reaches temperatures above 180 K almost all energy will be used to desorb water because of the energy losses by black body

radiation become small in comparison to the energy loss by desorption.

As mentioned above the high evaporation rate used above (e.g. $\Gamma \approx 9 \cdot 10^6 \text{ m}^{-3} \text{ s}^{-1}$) for the single intense maser spot given by Baudry & Diamond (1998) is much more difficult to explain: this evaporation rate is 3000 times higher than that assumed for the ground state masers. This high evaporation rate assumed for the 13.44 GHz maser can be explained qualitatively on the basis of the above discussion and the speculation that this maser is located very close to the star, e.g. at a distance of less than 200 AU. This speculation is based on the location of the maximum of the 23.8 GHz continuum map, where according to Baudry & Diamond (1998) the star is suspected to be. It is interesting to note that with this location of the star most of the $j = 3/2$ masers seem to be indeed at a distance of ≈ 1000 AU, where we assume the small grain border to be.

We assume, as before for the $j = 3/2$ masers, that the $j = 7/2$ maser is pumped by evaporation from water containing grains. In this case, however, the grains must have traveled from 1000 AU to 200 AU and still evaporate water. Therefore the “grains” must be very large because they survived the increasingly massive evaporation on their way towards the star. Because a time of roughly 800 years is required to travel the distance of 800 AU only very big “grains”, like comets or planets, survive this journey. We assume an average temperature of 200 K for a “grain” with radius 20 km approaching the star to estimate its life time. With the desorption flux $j_{\text{des}} = 2 \cdot 10^{22} \text{ m}^{-2} \text{ s}^{-1}$ at 200 K this yields a life time of ≈ 1600 years and at 800 AU the “grain” would still have a radius of 10 km. The situation described here is in closest analogy to comets that approach the sun and yield high water evaporation rates there.

At 200 AU, however, the temperature of this 10 km block can be considerably higher, in particular because the continuously increasing photolytic heating. Without any better knowledge we discuss an example with a temperature of 250 K for the 10 km block at 200 AU to explain the high evaporation rate of $\approx 10^7 \text{ m}^{-3} \text{ s}^{-1}$. With the desorption flux $j_{\text{des}} \approx 2.8 \cdot 10^{24} \text{ m}^{-2} \text{ s}^{-1}$ we obtain $O_{\text{gr}} \approx 3 \cdot 10^{-18} \text{ m}^2$ to explain this evaporation rate. Under the assumption of 10 km “grains” this requires a “grain” density $n_{\text{gr}} \approx 2.4 \cdot 10^{-27} \text{ m}^{-3}$.

This means that one block of 10 km radius is in a volume of $4 \cdot 10^{26} \text{ m}^3$ or an average distance between these blocks of $\approx 10^9 \text{ m}$. For this grain density a mass of $6.5 \cdot 10^{23} \text{ kg}$ is contained in the tubular maser volume of 20 AU^3 that was assumed above for the single intense 13.44 GHz maser spot by Baudry & Diamond (1998). With the mass $M \approx 2 \cdot 10^{23} \text{ kg}$ of Earth this implies that one third of the mass of earth is contained in the maser volume. For “grains” with $100\times$ higher porosity much less mass is required in the maser volume. These porous grains may survive the passage because of poor heat conduc-

tion to the inner part of the grain. Because the $j = 7/2$ masers are observed only once in the interstellar medium the somewhat exotic assumptions made here appear not to be too unreasonable.

One last remark is related to the probability for the appearance of a particular maser. This probability is determined not only by the gain but also by the probability for spontaneous emission, which clearly favours the excited state masers. On the other hand excited state masers require much larger evaporation rates than the ground state masers. Because these high evaporation rates are not available near the relatively cold border of the HII region the excited state masers should be much closer to the star where the heating of grains increases. The ground state masers on the other hand require neither high evaporation nor high photodissociation rates. If they are located at the border of the HII region they have long tube length and can nevertheless start even by spontaneous emission. Closer to the star, where the evaporation is high, the excited state masers may operate as amplifiers with e.g. the 20 mJy background radiation observed for the 13441 MHz maser.

4. Conclusions and summary

For the maser model presented above we used the generally accepted picture for star formation in which a massive new born B/O type star is surrounded by a HII region and a large surrounding cloud of dust. According to Bloemhof et al. (1996) some of the OH masers have “proper motions” and are falling towards the star. In this picture water containing grains move with considerable velocities of some km s^{-1} - depending on the distance from the star - towards the central star.

We defined a “small grain border” between the HII region and the cold interstellar cloud by the region where the small grains are directly irradiated by the heat flux from the star. The life time of these grains is short which implies that the “small grain border” should move outwards with time. Because the larger grains live longer than the small grains, the larger grains remain inside this border and are evaporated by the heat flux from the star in the presence of VUV radiation. They are photolysed and relax by IR radiation to lower states. The competition between photodissociation and IR relaxation yields a characteristic distribution over the OH quantum states which is determined by the competition between IR relaxation and photodissociation and does not depend on the evaporation rate.

Inversion and gain is found between all levels in the $^2\Pi_{3/2}$ multiplet for which OH masers are observed near new born stars which implies that all these observed OH masers can be explained by the photodissociation of water in the first absorption band. It is interesting to note that the masers do not require a high photodissociation rate

but operate over a wide range of γ 's. The gain for a given maser transition is the product of a specific gain and the evaporation rate for all OH quantum states. The specific gain results from the competition between the photodissociation rates and IR relaxation rates and is only a function of γ .

The specific gain is much larger for the ground state maser than for any of the excited state masers. Considerably large gains are obtained over a wide range of γ 's for the ground state and the gain increases with decreasing γ . This somewhat surprising result, i.e., that the inversion becomes large for small photodissociation rates, is due to the fact that the OH in the ground state is destroyed slowly for small γ 's which leads to a pile up of population in this state. Because of the large specific gain for the ground state relatively low evaporation rates are sufficient to obtain high gain. The evaporation of the 10 – 100 μm grains close to the border of the HII region yields sufficiently high evaporation rates even at low temperatures around 120 K. The grains also last a long time, so that they may be replaced by the grains moving from beyond the small grain border to the star or the ground state masers move with the velocity of the expanding HII region. Therefore the ground state masers can last for a long time.

In contrast to the ground state masers, the masers in the excited states suffer large losses due to IR relaxation and consequently show a much smaller specific gain. However, the specific gain is larger for small photodissociation rates and decreases with increasing γ . Because of the much smaller specific gain much larger evaporation rates are required to explain the high gains observed for excited states. To explain a gain of $3 \cdot 10^{-12} \text{ m}^{-1}$, as suggested by Baudry & Diamond (1998) for the $j = 7/2$ maser, the evaporation rate must become as high as $\Gamma \approx 10^7 \text{ m}^{-3} \text{ s}^{-1}$. This is only possible if many big “grains”, like comets or small planets, that live long enough to penetrate deep inside the HII region acquire high temperatures around e.g. 250 K. Then massive evaporation of water will occur and yield high evaporation rates which will, however, last only for a limited time. Some of the $j = 7/2$ maser spots observed by Baudry & Diamond (1998) et al. show indeed an intensity increase by a factor of more than 10 over a decade. The excited state masers are therefore expected to be transient phenomena during star formation.

There is much more work required to elucidate details of the present mechanism and there are other features of maser radiation that have to be explained, like line width,

velocity extent, variability or the fact that hyperfine lines appear sometimes in absorption and sometimes in emission. We believe that a deeper understanding of many of these features requires an extension of the present model, e.g. inclusion of FIR pumping and at very small γ 's collisional effects as well. Also, the situations near new born stars have to be compared in detail to analyse whether or not the predictions given here agree with observation.

Baudry & Diamond (1998) suspect that the central star is the “common source” of energy for the $j = 3/2$, $j = 5/2$ and $j = 7/2$ OH masers observed in W3(OH). This is exactly what results from the present model: the common source of energy is the heat- and VUV- flux that causes grains to evaporate water which is photolysed subsequently to give an inversion that depends also on IR relaxation. This yields high gain for all OH maser transitions observed near new born stars.

Acknowledgements. Most of the referenced papers used to develop the presented maser model are obtained using the *NASA Abstract Data System (ADS)*. We thank the NASA for this Service.

References

- Andresen P., 1985, *A&A* 154, 42
 Baudry A., Diamond P.J., 1998, *A&A* 331, 697
 Bloemhof E.E., Moran J.M., Reid M.J., 1996, *ApJ* 467, L117
 Combi M.R., Brown M.E., Feldmann P.D., et al., 1998, *AJ* 494, 816
 Destombes J.L., Marliere C., Baudry A., Brillet J., 1977, *A&A* 60, 55
 van Dishoeck E.F., Dalgarno A., 1984, *ApJ* 277, 576
 Elitzur M., 1992, *Astronomical Masers*. Kluwer
 Goorvitch D., Goldman A., Dothe H., Tipping R.H., Chackerian C. Jr., 1992, *J. Geophys. Research* 97, 20771
 Handbook of Chemistry and Physics, 1966, Weast R.C., Selby S.M. (eds.). The Chemical Rubber Co., Cleveland, Ohio
 Häusler D., Andresen P., Schinke R., 1987, *JCP* 87, 3949
 Nee J.B., Lee L.C., 1984, *JCP* 81, 31
 Schultz D., Li G.S.H., Scherb F., Roesler H.L., 1992, *Icarus* 96, 190
 Thissen T., Wurps H., Spiecker H., ter Meulen J.J., Andresen P. (submitted to *A&AS* Feb. 1999)
 Watanabe K., Zelikoff M., 1952, *J. Opt. Soc. Am.* 43, 753
 Wurps H., 1997, University of Bielefeld, PhD Thesis